

## Design and calibration of a semi-active control logic to mitigate structural vibrations in wind turbines

Nicola Caterino<sup>\*1,4</sup>, Christos T. Georgakis<sup>2a</sup>,  
Mariacristina Spizzuoco<sup>3b</sup> and Antonio Occhiuzzi<sup>1,4c</sup>

<sup>1</sup>Department of Civil Engineering, University of Naples "Parthenope", Centro Direzionale di Napoli, Isola C4, 80143, Naples, Italy

<sup>2</sup>Department of Civil Engineering, Technical University of Denmark (DTU), Building 118, 2800 Kgs. Lyngby, Denmark

<sup>3</sup>Department of Structures for Engineering and Architecture, University of Naples Federico II, via Claudio 21, 80125, Naples, Italy

<sup>4</sup>Construction Technologies Institute, National Research Council (CNR), Viale Lombardia, 49, 20098, San Giuliano Milanese (MI), Italy

(Received September 26, 2015, Revised April 21, 2016, Accepted May 6, 2016)

**Abstract.** The design of a semi-active (SA) control system addressed to mitigate wind induced structural demand to high wind turbine towers is discussed herein. Actually, the remarkable growth in height of wind turbines in the last decades, for a higher production of electricity, makes this issue pressing than ever. The main objective is limiting bending moment demand by relaxing the base restraint, without increasing the top displacement, so reducing the incidence of harmful "p-delta" effects. A variable restraint at the base, able to modify in real time its mechanical properties according to the instantaneous response of the tower, is proposed. It is made of a smooth hinge with additional elastic stiffness and variable damping respectively given by springs and SA magnetorheological (MR) dampers installed in parallel. The idea has been physically realized at the Denmark Technical University where a 1/20 scale model of a real, one hundred meters tall wind turbine has been assumed as case study for shaking table tests. A special control algorithm has been purposely designed to drive MR dampers. Starting from the results of preliminary laboratory tests, a finite element model of such structure has been calibrated so as to develop several numerical simulations addressed to calibrate the controller, i.e., to achieve as much as possible different, even conflicting, structural goals. The results are definitely encouraging, since the best configuration of the controller led to about 80% of reduction of base stress, as well as to about 30% of reduction of top displacement in respect to the fixed base case.

**Keywords:** semi-active control; wind turbine; magnetorheological damper; control algorithm

---

\*Corresponding author, Assistant Professor, E-mail: [nicola.caterino@uniparthenope.it](mailto:nicola.caterino@uniparthenope.it)

<sup>a</sup> Professor, E-mail: [cg@byg.dtu.dk](mailto:cg@byg.dtu.dk)

<sup>b</sup> PhD, E-mail: [spizzuoc@unina.it](mailto:spizzuoc@unina.it)

<sup>c</sup> Professor, E-mail: [antonio.occhiuzzi@itc.cnr.it](mailto:antonio.occhiuzzi@itc.cnr.it)

## 1. Introduction

Wind turbines generally involve complex structural issues in the context of natural wind due to interaction of the rotating blades and the tower. High wind loads can cause the system to leave the normal operation, eventually with local or extensive structural damage. To prevent such failures during operation, a safety supervisor (Pedersen 2012) is generally installed to trigger an emergency shutdown prior to any component being damaged. A solution widely adopted to protect such structures consists in monitoring the rotational speed of the turbine, then commanding the shutdown of the system when a given threshold is exceeded (Wisniewsky *et al.* 2013). A typical emergency shutdown is based on the aerodynamic braking principle, slowly pitching the blades to  $90^\circ$  and turning off the generator torque. Some wind turbines also implement mechanical brakes to assist in the emergency shutdown. However, shutdown is an undesired action because of the social/economic consequences. Wind energy is more and more integrated into the utility networks of the leading countries and disruptions may be very costly. For such reasons, much research of the last years about wind energy has been devoted to improve the structural safety of large wind turbines while limiting as much as possible the number of emergency shutdowns. Herein the studies addressed to investigate different techniques to reduce structural demand imposed to high tower by extreme wind loads are focused. The scientific literature on this topic is mainly related to passive control strategies, but also some preliminary ideas about active or semi-active (SA) control techniques have been recently proposed.

Most of the passive techniques in literature to mitigate structural vibrations of wind turbines are based on the use of tuned mass dampers (TMDs), sometimes realized by means of a liquid mass, rather than solid. Murtagh *et al.* (2008) propose the installation of a TMD at the top of the tower and analyze the dynamic response of a coupled blades-tower-damper system under the action of two different rotationally sampled wind turbulences. Numerical simulations show that the optimal tuning of the dampers allowed a reduction of maximum tip displacement of about 20% in respect to the uncontrolled case. Colwell and Basu (2009) present an offshore wind tower equipped with a passive tuned liquid column damper (TLCD) that leads to a reduction up to 55% in the peak response of the tower subjected to wind and wave excitations. Rodríguez *et al.* (2011) explore the possibility of integrating passive viscous dampers in a toggle-brace assembly within the hollow column of the tower, able to give a reduction of base bending moment for extreme and fatigue loads up to 20% and 10% respectively. Li *et al.* (2012) evaluate the effectiveness of a ball vibration absorber (BVA) in reducing structural demand through shake table tests on a 1/3 scaled model under wind-wave equivalent loads and ground motions. The passive device installed on the top of the nacelle allowed a response reduction, in terms of top displacement, top acceleration and bottom stress of the wind turbine tower, variable from 15% to 53%. Afterward, Zhang *et al.* (2013) developed a nonlinear analytical model of such BVA-controlled wind turbine system, calibrated with reference to the above experimental outcomes, to further investigate such control technique. Chen and Georgakis (2013) performed an experimental analysis of a 1/20-scale wind tower model equipped with a passive rolling-ball damper. The latter consists of a glass container placed at the top of the model and having one or more steel balls inside. Different configurations have been tested, changing the geometry of the container (one or two layers) and the number of balls (one to six), showing a significant reduction of the peak value and standard deviation of top displacement and base bending moment. The same authors (2015) tested the same model using water rather than steel balls inside the glass container, i.e., realizing a spherical tuned liquid damper. The optimal degree of filling with water (1-2% of the total generalized mass of the system) has been found for

the maximum reduction of structural demand. Passive structural control was also presented by Enevoldsen and Mørk (1996), who investigate the effect of passive damping on a 40 m high and 500 kW pitch regulated three-bladed horizontal wind turbine. Bortoluzzi *et al.* (2015) discuss the theoretical aspects and formulate a design process for TMD solution to mitigate wind-induced local vibrations. Dinh and Basu (2015) investigate the use of single and multiple TMDs for passive control of edgewise vibrations of nacelle/tower and spar of spar-type floating wind turbines (S-FOWTs). Uncontrolled and controlled mathematical models of the S-FOWT are developed by using Euler-Lagrangian energy formulations, showing that a single TMD can reduce up to 40% of the nacelle sway displacement and the spar roll, and that the reduction observed with multiple TMDs is 50%. Basu *et al.* (2014) propose a possible numerical model to reproduce mechanical and structural vibrations in wind turbines due to the occurrence of electrical faults and an effective means of suppressing the vibrations with flexible alternating current transmission systems (FACTS) devices. Two types of FACTS devices have been studied, namely a static synchronous compensator and a unified power quality conditioner, demonstrating remarkable capability of both in suppressing blade in plane or edgewise vibrations, tower/nacelle accelerations and drivetrain oscillations. Recent advances about procedures for the optimal tuning of passive TMD to reduce structural demand for first-mode dominated structures against several types of external excitation are shown by Salvi and Rizzi (2016).

About active/semi-active control strategies from literature related to wind turbines, Karimi *et al.* (2010) and Luo *et al.* (2011) propose a SA control technique for floating wind turbines with TLCD. This device, generally used as a passive damper, turns into a SA device using a controllable valve. The orifice opening is real time adapted according to the structure response and loading conditions, with a control logic based on a  $H_\infty$  feedback methodology. Lackner and Rotea (2011) investigate the effectiveness of an optimal passive TMD and of a hybrid mass damper (HMD, i.e. a TMD improved with the addition of a controlled force actuator) in reducing fatigue loads due to bending moment at the base of the tower, showing a percentage reduction of about 10% and 30% respectively due to each of the two proposed systems.

Kirkegaard *et al.* (2002) have been the first to explore the use of magnetorheological (MR) dampers to control a wind turbine, assuming such type of smart device to be installed, in a vertical position, between the base and the top of the tower. Even hard to be implemented in a real case, the numerical simulations show good results. Experimental results are also made available by the authors, unfortunately referred to the passive use (constant voltage fed to the MR damper) of the device only.

The authors of the present research recently proposed a SA control technique based on the use of MR devices to realize a time-variant base restraint whose “stiffness” can be in real time driven by a purposely written control logic (Caterino *et al.* 2014, Caterino 2015). The controller can be programmed to instantaneously calibrate the MR devices installed at the base of the tower. In this way the base bending moment can be reduced, in selected intervals of time, by relaxing the base restraint. Secondly the control logic has to hold the top displacement within acceptable values so as to avoid significant, detrimental second order effects.

An experimental setup to perform shaking table tests of a wind turbine tower model semi-actively controlled as above has been recently realized by the authors at the laboratory of the Denmark Technical University (DTU) in Copenhagen. The results of a preliminary campaign are described in the two papers above and show high potential for such innovative control strategy in reducing the structural demand of base stress, at the cost, in the worst case, of a slight increase of top displacement.

This work intends to formalize the above idea, trying to provide additional tools and information useful to implement applications of the proposed SA control system to real cases as well as allowing to plan a second series of tests with the setup available at the DTU. Starting from the results of the tests above, a finite element (FE) model of the structure has been calibrated so as to develop several numerical simulations addressed to calibrate the control logic designed for such kind of applications. The final results are strongly encouraging, since the best configuration of the controller led to about 80% of reduction of base stress, as well as to about 30% of reduction of top displacement in respect to the fixed base case.

## 2. A variable base restraint for wind turbine towers. Control algorithm

A smart base restraint suitable for wind turbine towers is proposed with the aim of reducing wind induced structural demand. The system is based on the use of controllable fluid based devices. The idea is schematically below, where the uncontrolled wind turbine in Fig. 1(a), fully restrained at the base, is modified as in Fig. 1(b). In other words, the perfectly rigid base restraint is replaced by a controllable, able to become more or less “stiff” during the motion, according to the instantaneous response of the tower. Fig. 1(b) sketches how it is possible to materialize this idea, that is installing at the base of the tower a smooth hinge, a rotational spring (of stiffness  $k_\phi$ ) and a rotational variable damper whose damping constant  $c_\phi$  can be driven in real time by a control algorithm.

SA MR dampers are smart devices suitable for the proposed control system. Varying the MR dampers’ properties according to a given control logic, the base control system is able to realize a real time regulation of the system’s stiffness. When a low value is imposed to the base damping, the base restraint is less “stiff”, so that the structure is able to relax by converting its potential energy into kinetic energy. In such cases, bending moment at the base is reduced. An undesired consequence could be the increase of top displacement demand, related to both the rigid body motion associated to the base rotation and the elastic deflection of the tower. The SA control algorithm has to limit this effect, i.e., it has to bound top displacements within acceptable value, so reducing the incidence of harmful second order effects.

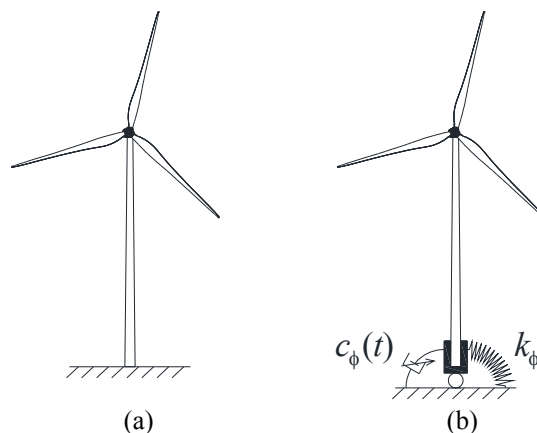


Fig. 1 Conventional structural scheme (a) and proposed idea of variable base restraint and (b) for a wind turbine

Predefined control algorithms for such specific application are not available in literature, where much more space is dedicated to SA controllers for seismic protection of structures, still based on the use MR dampers. A specific control algorithm, based on a simple, physical approach, has been formulated and fully described by the authors in Caterino *et al.* (2014). It is a bang-bang controller, switching back and forth from an “off” state (intensity of current  $i = i_{\min}$ , i.e. the minimum current set to be given to the dampers) to an “on” state ( $i = i_{\max}$ , i.e. the maximum assumed value for the current) according to a logic aiming to control both base stress and top displacement. In other words, the control algorithm was developed aiming to achieve a trade-off between the two contradictory objectives of limiting maximum values of base stress and of top displacement within given limits, namely  $\sigma_{\lim}$  and  $x_{\lim}$ , respectively. Its logic is described in Eq. (1), where  $\sigma(t)$ ,  $x(t)$  and  $\dot{x}(t)$  are respectively the value of stress at the base, top displacement and top velocity at the instant of time  $t$ .

$$\begin{aligned}
 \text{a) if } |\sigma(t)| < \sigma_{\lim} & \rightarrow i(t) = i_{\max} \\
 \text{b) if } |\sigma(t)| \geq \sigma_{\lim} \text{ and } |x(t)| < x_{\lim} & \rightarrow i(t) = 0 \\
 \text{c) if } |\sigma(t)| \geq \sigma_{\lim} \text{ and } |x(t)| \geq x_{\lim} \text{ and } x(t) \cdot \dot{x}(t) > 0 & \rightarrow i(t) = i_{\max} \\
 \text{d) if } |\sigma(t)| \geq \sigma_{\lim} \text{ and } |x(t)| \geq x_{\lim} \text{ and } x(t) \cdot \dot{x}(t) \leq 0 & \rightarrow i(t) = 0
 \end{aligned} \tag{1}$$

Therefore, the controller makes “stiffer” (dampers to on) the base restraint until the stress exceeds the limit value  $\sigma_{\lim}$ , whereas “relaxes” it (off) when this limit is overpassed and the displacement is still acceptable (i.e., less than  $x_{\lim}$ ). When both stress and displacement are beyond the respective threshold values, the controller switches on the dampers if the displacement is going towards a larger value (so trying to damp or invert the displacement’s trend; see expression c) of Eq. (1)), otherwise it switches off the MR devices to make them collaborating to both stress and displacement reduction. Fig. 2 schematically describes the above defined logic. The decision of the controller (switch on or switch off) depends on the occurrence of each of the four possible combinations regarding the value of base stress, top displacement, and top velocity.

The application of the proposed control algorithm requires the definition of rational criteria to calibrate the parameters involved in, that is  $i_{\min}$ ,  $i_{\max}$ ,  $\sigma_{\lim}$  and  $x_{\lim}$ . Herein a wide numerical campaign has been performed with reference to a case study structure, aiming to investigate the role each parameter has regarding the structural response, and to learn how to calibrate them to achieve the maximum reduction of stresses and displacements.

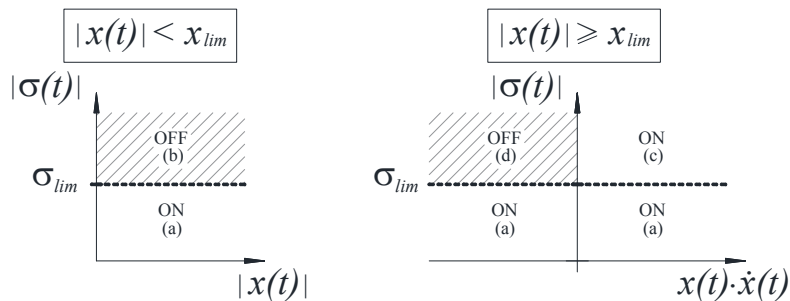


Fig. 2 The logic behind the controller (symbols refer to Eq. (1))

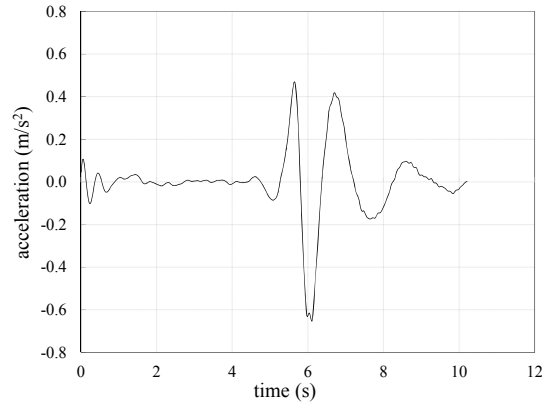


Fig. 3 Equivalent base acceleration time history for the selected wind load case

### 3. Operative procedure to calibrate the SA controller. A case study.

A calibration procedure for the above SA control algorithm is herein proposed. The first step consists in generating a FE model of the structure, able to simulate both fixed base (FB) and SA controlled configurations. Then, with reference to a given wind load, the structural response in the FB case has to be determined. Several SA numerical simulations then have to be performed, each time assuming a different value of each of the above parameters, within predefined ranges. Analyzing the results allows to single out the configuration of the controller able to achieve the maximum reduction of base stress while not causing increasing of top displacement in respect to the FB case. This procedure is practically applied in the following with reference to a specific case study.

#### 3.1 Case study

The case study structure is a 1/20-scale structural model of a prototype real wind turbine. The reference real structure is a 3 MW wind turbine with horizontal power transmission axle, 102.4 m tall, with a variable hollow circular cross section whose external diameter is variable from 2.30 m (top) to 4.15 m (bottom). Chen and Georgakis (2013) demonstrated its dynamic equivalence (in terms of equivalent flexural stiffness) with a single degree of freedom (SDOF) structural system made up of a tapered tubular cantilever beam with a concentrated mass at the top. The scaled structure is characterized by a 5.12 m high vertical tube with uniform cross section  $\Phi 133/4$  (133 mm is the external diameter, 4 mm the thickness), and a lumped mass of 280 kg placed at the top.

The above structural model has been realized at the laboratory of the DTU and fully described in Caterino *et al.* (2014). Herein the description is summarized, for the convenience of the reader. The base of the model is highly stiff and is supported in the middle by a cylindrical steel hinge. On both sides of the base, one cylindrical spring and one MR damper are installed. The assembly “elastic springs + SA MR dampers”, placed in parallel at the base of the tower, just represents the smart base restraint herein proposed to control the dynamic behavior of the structure.

An extreme operating gust loading has been considered as reference wind action: a sharp

increase, then decrease in wind speed within a short period of time. Chen and Georgakis (2013) defined an equivalent base acceleration time history (Fig. 3), that is the base input that would provide the same top mass response of the real fixed base structure subjected to the wind action. This kind of analysis was made using the wind turbine aeroelastic code HAWC2 (Horizontal Axis Wind turbine simulation Code, 2<sup>nd</sup> generation), realized at the DTU for calculating wind turbine response in time domain (Larsen and Hansen 2008).

### 3.2 Numerical model

A FE model has been generated in Matlab environment to simulate the dynamic behavior of the case study structure. It consists in 37 elements. A number of 36 elements simulate the tower with uniform diameter (133 mm) and thickness (4 mm) along the height, while the last element (37<sup>th</sup>) is more rigid and represents the connection of the top of the tower to the barycenter of the nacelle. The rotor and the aerodynamics have not been included in the model due to its complexity. The nacelle and its internal components are represented by a concentrated mass at the top of the structure, neglecting their dynamic interaction.

The base support has been modeled as in Fig. 4, that is by a rotational spring  $k_{\text{spring}}$  and a Maxwell element (representing the MR dampers) working in parallel. The value for  $k_{\text{spring}}$  (7.5e4 Nm/rad) has been derived from the experimental setup, known the stiffness (89 kN/m) of the two linear springs and their distance from the center of rotation (0.65 m). The Maxwell element, as known, consists of a spring  $k_{\text{Maxwell}}$  and a linear viscous damper  $c_{\text{Maxwell}}$  in series. The controllable part of this device is represented by the constant  $c_{\text{Maxwell}}$ , while  $k_{\text{Maxwell}}$  has been simply assumed high enough (1.5e6 Nm/rad) so as to behave like a rigid link. Two different values of  $c_{\text{Maxwell}}$  ( $c_{\text{on}}$ ,  $c_{\text{off}}$ ) have been determined so as to reproduce the dissipative capability of MR dampers respectively in the on and off states. These two opposite configurations of the MR dampers are assumed to be similar to those of the experimental campaign cited above, respectively corresponding to  $i=i_{\text{min}}=0$  A and  $i=i_{\text{max}}=1$  A. The MR dampers considered to calibrate the Maxwell device properties are those adopted for the laboratory tests at DTU also. Suitable numerical models for such devices are described by Caterino *et al.* (2011). The values of  $c_{\text{on}}$ ,  $c_{\text{off}}$  have been derived starting from this study, further calibrated so as to reproduce as much as possible the experimental response registered during the tests at the DTU laboratory. Finally they resulted to be  $c_{\text{on}}=1e7$  Nms/rad and  $c_{\text{off}}=2e3$  Nms/rad.

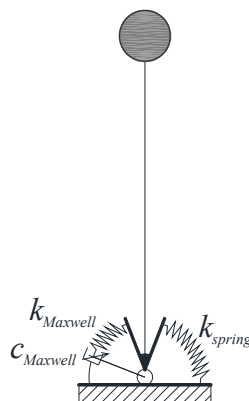


Fig. 4 Representation of the base restraint within the FE model of the SA controlled structure

Table 1 Modal information for FB, Passive-on, and Passive-off structural schemes (1<sup>st</sup> mode)

<i>Model</i>	<i>f</i> (Hz)	<i>T</i> (s)	(-)
Fixed Base	0.94	1.06	2.0 %
Passive-on	0.85	1.17	2.5 %
Passive-off	0.40	2.52	7.4 %

The modal analyses respectively performed with reference to the FB model, to the SA model with  $c(t)=\text{constant}=c_{\text{on}}$  (“passive-on” mode) and to the SA model with  $c(t)=\text{constant}=c_{\text{off}}$  (“passive-off” mode) led to the results summarized in Table 1 where frequency  $f$ , period  $T$  and damping ratio  $\xi$  are referred to the fundamental mode. As expected, the FB and the passive-on cases are similar, while the passive-off configuration, allowing more base rocking, corresponds to a longer period of vibration and to more structural damping.

A customized integration procedure based on the Newmark’s approach has been formulated for the analyses. The action of the MR damper is modeled separately, as external control moment applied at the base of the tower. The integration procedure is based on forward and backward differences, which yield to the base bending moment. In order to simulate the time delay in the mechanical response of the MR dampers, each on/off and off/on switch is imposed to occur not instantaneously, rather in ten milliseconds (Caterino *et al.* 2013) by following a linear law.

### 3.3 Preliminary numerical/experimental comparisons

About preliminary experimental activity done with reference to the above mock-up structure, the reader should refer to Caterino *et al.* (2014) for details. The model has been tested first in FB configuration, then in the case of SA control. Table 2 resumes the peak values of the response for both cases. The SA test has been performed using, as combination of limit values ( $\sigma_{\text{lim}}$ ,  $x_{\text{lim}}$ ), the couple (30 MPa, 45 mm) selected since corresponding to 60% of the maximum base stress registered in FB experimental condition, with an acceptable increase of the top displacement within 15% with respect to the FB experimental result. Table 2, Figs. 5 and 6 allow a direct comparison of numerical and experimental results, in terms of peak values of the response as well as of time-history sequences of data for top displacement, base stress and MR command voltage.

The numerical model seems to be able to reproduce the global behavior of the structure, leading to results that are in good agreement with those experimentally measured in laboratory, for both FB (Fig. 5) and SA (Fig. 6) cases. Actually, the numerical model could be refined to lead to a better matching of numerical and experimental data. Authors decide to postpone this task until a new experimental campaign, programmed to be done in the near future, will be actually performed. This because the data registered during the preliminary laboratory tests are characterized by some approximations that, in the next campaign, will be avoided so to make more reliable the registered data. During the first tests, base stress and top displacement were not directly measured, rather on line derived from measurements, via laser transducers, assuming the structure is totally 1<sup>st</sup> mode dominated and that it behaves elastically during the whole motion.

Anyway, from a more general point of view, the above numerical outcomes, despite an improvable superposition of experimental and numerical data, clearly confirm the validity of the FE model as a tool suitable to perform the numerical analyses object of the present study, i.e. to

gather information about the sensitivity of the structural response to the different configurations of the SA control algorithm.

#### 4. Numerical simulations: results and discussion

A number of 100 numerical tests have been performed with reference to the above FE model in SA configuration. This is the total number of different combinations of stress ( $\sigma_{lim}$ ) and displacement ( $x_{lim}$ ) limits that have been tested, respectively chosen within the range [5, 50] MPa, with a step of 5 MPa, and within the range [5, 50] mm, with a step of 5 mm. The upper bound of the above ranges have been defined so as to be close to the values representing the FB response (Table 2). The steps 5 MPa and 5 mm have been chosen trading off the need of covering the range with a large enough points and that of limiting the computational effort.

The main results of such a wide numerical campaign are presented and discussed in the following. Performance indices have been assumed to quantitatively summarize the structural response in the examined cases. These allow to compare the effectiveness of the SA control strategy for each of the above settings for the controller, then to select the optimal calibration of the latter. The indices, and relative symbols, are:

- maximum bending stress at the base of the tower ( $\sigma_{max}$ );
- maximum top displacement ( $x_{max}$ );
- ratio of  $\sigma_{max}$  to the value of  $\sigma_{lim}$  assumed to calibrate the controller ( $\sigma_{max} / \sigma_{lim}$ );
- ratio of maximum bending stress in SA to FB conditions ( $\sigma_{max} / \sigma_{max,FB}$ );

Table 2 Numerical and experimental peak values for  $\sigma$  and  $x$ , for the FB and SA cases

Case		$\sigma_{max}$ (MPa)	$x_{max}$ (mm)
Experimental	FB	51	39
	SA	36	45
Numerical	FB	54	41
	SA	32	37

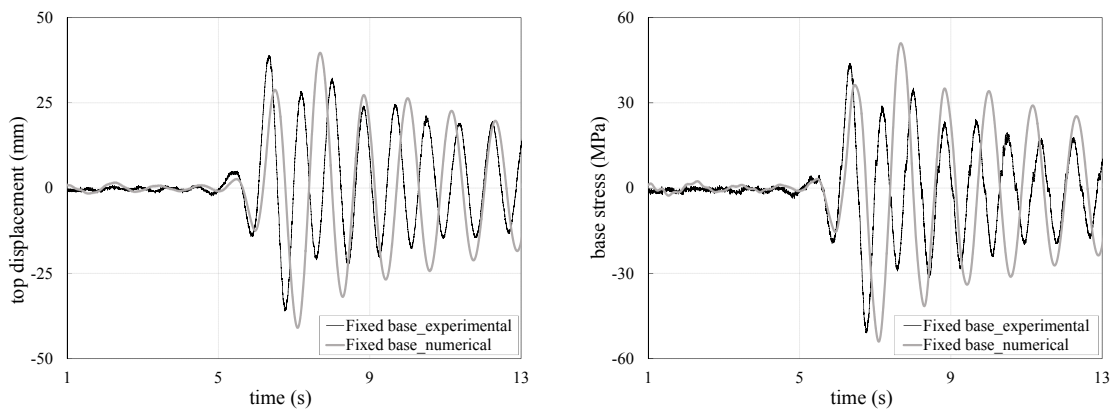


Fig. 5 Fixed base test: numerical versus experimental results

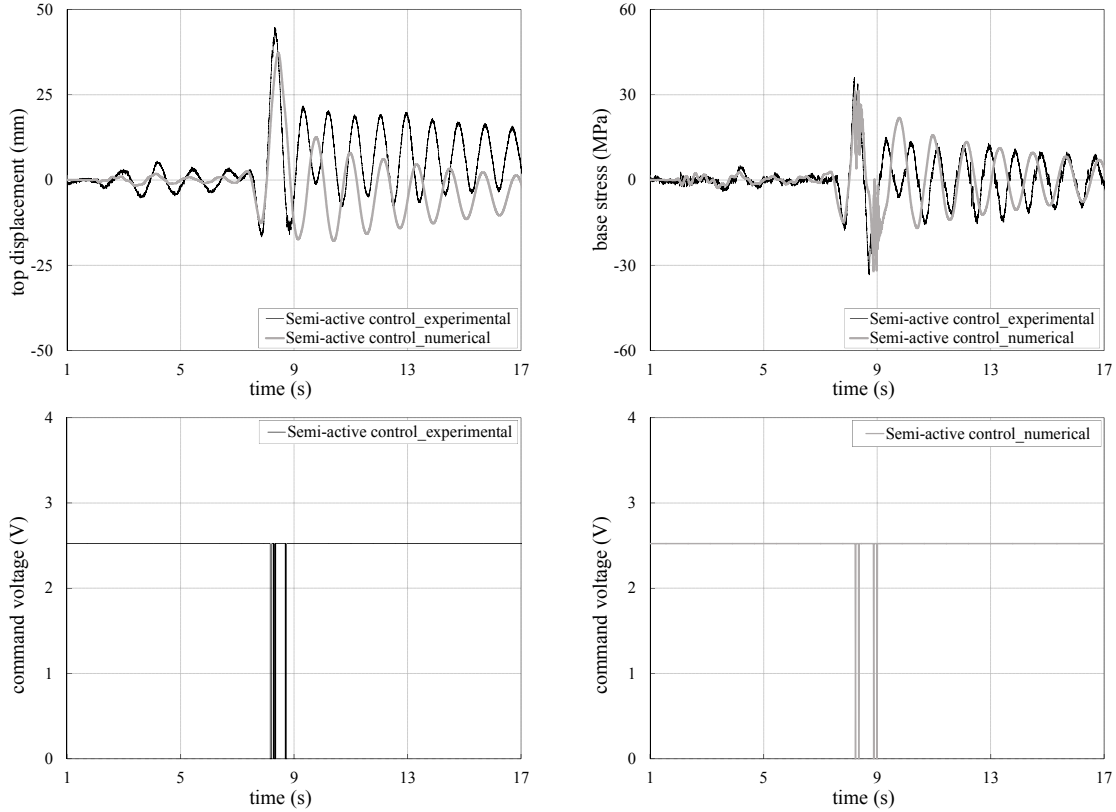


Fig. 6 Semi-active controlled tests (limits 30 MPa, 45 mm): numerical versus experimental results

- ratio of maximum top displacement in SA to FB conditions ( $x_{\max} / x_{\max,FB}$ );

Moreover, to better interpret the results, the following two additional information have been gathered from each numerical simulation performed:

- total amount of time in which the MR damper has been switched off by the controller ( $t_{\text{off}}$ );
- total number of switches (on $\rightarrow$ off and vice versa) commanded to the variable device ( $n_{\text{sw}}$ ).

The ratio  $\sigma_{\max} / \sigma_{\text{lim}}$  allows to check if and how the controller has been able to limit the bending stress to the desired value  $\sigma_{\text{lim}}$ . In the ideal case, this ratio should be less than or equal to one. It is worth noting that the ratio  $x_{\max} / x_{\text{lim}}$  is not significant to the same extent given that  $x_{\text{lim}}$  has a reduced impact on the controller operation. For this reason, it has not been assumed as parameter for comparison. The indices  $\sigma_{\max} / \sigma_{\max,FB}$  and  $x_{\max} / x_{\max,FB}$  express the effectiveness of the controller in reducing the structural response with respect to the FB conditions. Values less than one are desired, since they reflect the main purpose of the control strategy. Values greater than one denote undesired structural performances in SA conditions, worse than in the uncontrolled FB case.

The indices  $t_{\text{off}}$  and  $n_{\text{sw}}$  give a quantitative idea about the activity of the MR damper during each

test. When the smart device is set to on, it is not very far from acting as a rigid link. Therefore, the above  $t_{\text{off}}$  gives also a measure of the overall duration of the dissipation phase.

The 100 different configurations of the controller are assessed in the following according to the above indicators. This allows to deeply understand the role of the involved parameters in the operation and effectiveness of the controller. After that, the numerical calibration of the controller, i.e., the selection of the best combination of  $\sigma_{\text{lim}}$  and  $x_{\text{lim}}$  values, among those examined, is performed according to Eq. (2). The latter aims to achieve the greatest reduction of the base stress (objective function) and, at the same time, a top displacement (constraint function) no higher than that in uncontrolled FB conditions

$$\min(\sigma_{\text{max}} / \sigma_{\text{max, FB}}) \quad \text{subject to} \quad x_{\text{max}} / x_{\text{max, FB}} \leq 1 \quad (2)$$

The following graphs depict the main results of the numerical analyses performed. The indicators in Fig. 7 show the values for the 100 case of analyses actually done. Then adjacent indicators of the same set of data are joined by a dashed line, however only to more clearly show the trend of each series as a function of  $\sigma_{\text{lim}}$ . It is worth noting that  $t_{\text{off}}$  and  $n_{\text{sw}}$  resulted to be only marginally dependent on the assumed value of  $x_{\text{lim}}$ , so Fig. 7(f) shows how these parameters changes according to  $\sigma_{\text{lim}}$ , considering the mean value among the ones corresponding, for a given value of  $\sigma_{\text{lim}}$ , to the 10 values of  $x_{\text{lim}}$  examined.

Analyzing diagrams (a) to (d) in Fig. 7, it emerges that the SA control applied to the case study wind turbine is always beneficial in terms of reduction of base stress with respect to the FB scheme, regardless of the special configuration for the controller. As expected, this is not confirmed regarding the response in top displacement, that in some cases exceeds the reference  $x_{\text{max, FB}}$  value. Considered the whole set of cases examined within the numerical investigation, the maximum base stress reduction results to be around 80%, and corresponds to the case  $(\sigma_{\text{lim}}, x_{\text{lim}})=(5 \text{ MPa}, 25 \text{ mm})$ . The maximum top displacement reduction is about 35%, for  $(\sigma_{\text{lim}}, x_{\text{lim}})=(10 \text{ MPa}, 15 \text{ mm})$ . The worst case, i.e. that corresponding to the maximum amplification of  $x$  (+40%) with respect to the FB case is  $(\sigma_{\text{lim}}, x_{\text{lim}})=(35 \text{ MPa}, 50 \text{ mm})$ .

Higher operation of the SA controller for smaller value of  $\sigma_{\text{lim}}$ , as expected, can be deduced from Fig. 7(f). Fig. 7(e) instead highlights that response values in terms of maximum base stress  $\sigma_{\text{max}}$  are practically always included in the interval  $[\sigma_{\text{lim}}, 2\sigma_{\text{lim}}]$ , with the exception of those cases where both very small values are fixed both for  $\sigma_{\text{lim}}$  and  $x_{\text{lim}}$ . This demonstrates the effectiveness of the controller, in most of the configurations, in reducing the response according to what is the intent expressed by the user assuming a specific value for  $\sigma_{\text{lim}}$ .

The trend of variability of  $\sigma_{\text{max}}$  according to the assumed value for  $\sigma_{\text{lim}}$  is roughly monotonic: the smaller the assumed value for  $\sigma_{\text{lim}}$ , the smaller the recorded value of  $\sigma_{\text{max}}$ , the value of the latter also being dependent on the value set for  $x_{\text{lim}}$  (Fig. 7(a)).

The same trend is not detected for  $x_{\text{max}}$  Fig. 7(b), where the response fluctuates around the value (41 mm) registered for the FB case. Actually, about half (53%) of the examined configurations of the controller led to undesired response in top displacement, i.e. values of  $x_{\text{max}}$  larger than  $x_{\text{max, FB}}$ . Fig. 8 explicitly highlight (with empty circles) what are the combinations of limit values  $\sigma_{\text{lim}}$  and  $x_{\text{lim}}$  giving undesired response in displacement. Looking at both Fig. 7 and Fig. 8, it results that, when values of  $\sigma_{\text{lim}}$  greater than 30 MPa are adopted (i.e. roughly greater than half of the  $\sigma_{\text{max, FB}}$  value), there is no chance to reduce displacements in respect to the FB case. The reason is related to the fact that in such cases the SA operations are really limited, as from Fig. 7(f) clearly

emerges. Therefore, the dissipation phases are concentrated in much small intervals of time, not effective in reducing significantly the response in displacement. In such cases, the effect related to the instantaneous relaxing of the base restraint, as this is not accompanied by a significant dissipation of energy, predominates so as to lead to top displacement values even 40% greater than in the FB condition. Vice versa, when smaller values of  $\sigma_{lim}$  are used ( $< 30$  MPa), the reduction or amplification of  $x_{max}$  in respect to  $x_{max,FB}$  also depends on the assumed value for  $x_{lim}$ . Also in this case, it seems that selecting values for  $x_{lim}$  less than  $0.5x_{max,FB}$  leads always to good results in terms of displacement response.

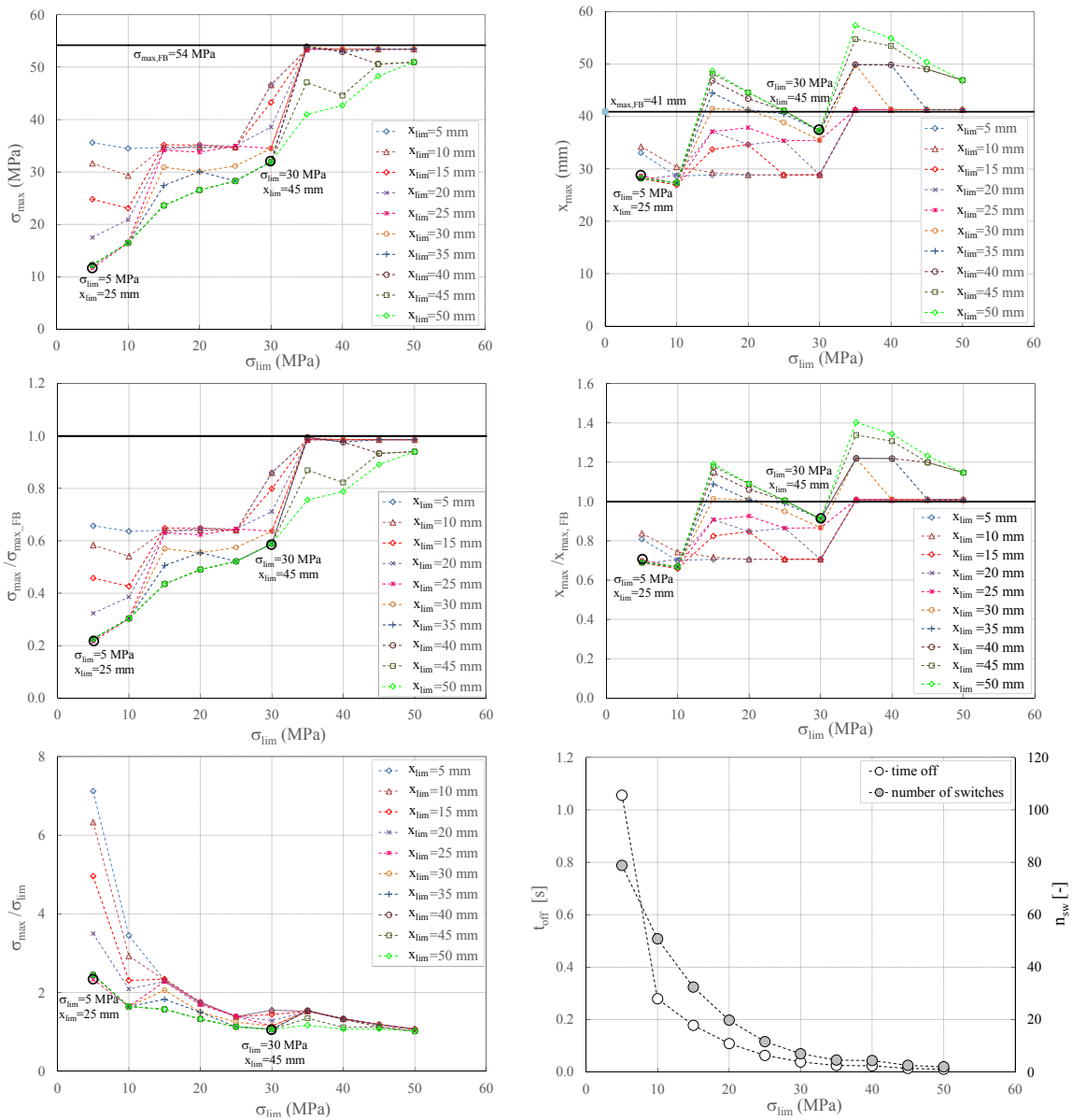


Fig. 7 Performance indices for the 100 configurations tested for the SA controller

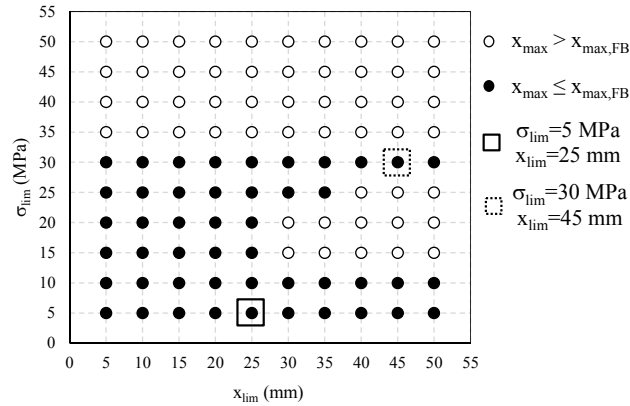


Fig. 8 Configurations of the controller corresponding to acceptable (black filled circle) and excessive (empty circle) top displacement response

According to the criterion defined in Eq. (2), the best configuration of the control algorithm results to be  $(\sigma_{lim}, x_{lim})=(5 \text{ MPa}, 25 \text{ mm})$  since it leads to the maximum response reduction (about 80%) in base stress, and also to a reduction (about 30%) of displacement in respect to the FB case. Therefore, preliminary conclusions about a possible way to calibrate the controller lead to suggest to assume values of  $\sigma_{lim}$  and  $x_{lim}$  respectively around  $0.1\sigma_{max,FB}$  and  $0.5x_{max,FB}$ .

In the previous Figs. 7 and 8, the results corresponding to two specific configurations of the control algorithm have been highlighted: the case  $(\sigma_{lim}, x_{lim})=(30 \text{ MPa}, 45 \text{ mm})$  and the case  $(\sigma_{lim}, x_{lim})=(5 \text{ MPa}, 25 \text{ mm})$ . The first one reflects the configuration of the experimental test cited in the previous section, the second one is that resulted to be the optimal configuration according to the criterion in Eq. (2). As said in Section 3.3, the calibration adopted for the experimental test was defined so as to aim at a 40% reduction of the base stress in respect to the FB condition, at the same time tolerating an increase of the top displacement however not higher than 15%. Reducing even more the base stress in the lab was considered too risky, as far the expected consequence on the displacement response was concerned. Numerical simulations now confirmed that, for moderately lower values of  $\sigma_{lim}$  (i.e., 15, 20, 25 MPa; see Figs. 7(b) and 7(d)), larger top displacements occur, even higher than in the FB condition. However, what these simulations also show, hardly predictable before, is a trend reversal for values of  $\sigma_{lim}$  even more smaller (i.e., 5, 10 MPa). In these cases, the significant reduction of base stress is further accompanied by a reduction of the top displacement also. This is due to the higher operation of the controller and, therefore, to the drastic increase of dissipated energy due to the rocking of the base.

The following Figs. 9 and 10 allow to further explore such aspects. They show the time history response of the structure when controlled with the above parameters  $(\sigma_{lim}, x_{lim})=(30 \text{ MPa}, 45 \text{ mm})$  and  $(\sigma_{lim}, x_{lim})=(5 \text{ MPa}, 25 \text{ mm})$ , also comparing them with the FB response. The quick modifications of base stress in some time intervals are associated to the intense activity of the controller, i.e., to the numerous (for unit of time) switches on/off and off/on, when the response stress value moves around the established limit value. This effect is more evident for stress, rather than for displacement, since the instantaneous change of the base restraint mechanical behaviour has more direct consequences on the bending moment at the bottom of the tower.

The better performance of the controller when calibrated with  $(\sigma_{lim}, x_{lim})=(5 \text{ MPa}, 25 \text{ mm})$  can also be justified observing Fig. 10(c). The above configuration leads to a much more intense activity of the controller, therefore to larger and more frequent rotations of the base, finally to a higher dissipation of energy. Moreover Figs. 10(a) and 10(b) show a larger number of non-linear loops  $(x, \sigma)$  for the case  $(\sigma_{lim}, x_{lim})=(5 \text{ MPa}, 25 \text{ mm})$  compared with that obtained with  $(\sigma_{lim}, x_{lim})=(30 \text{ MPa}, 45 \text{ mm})$ .

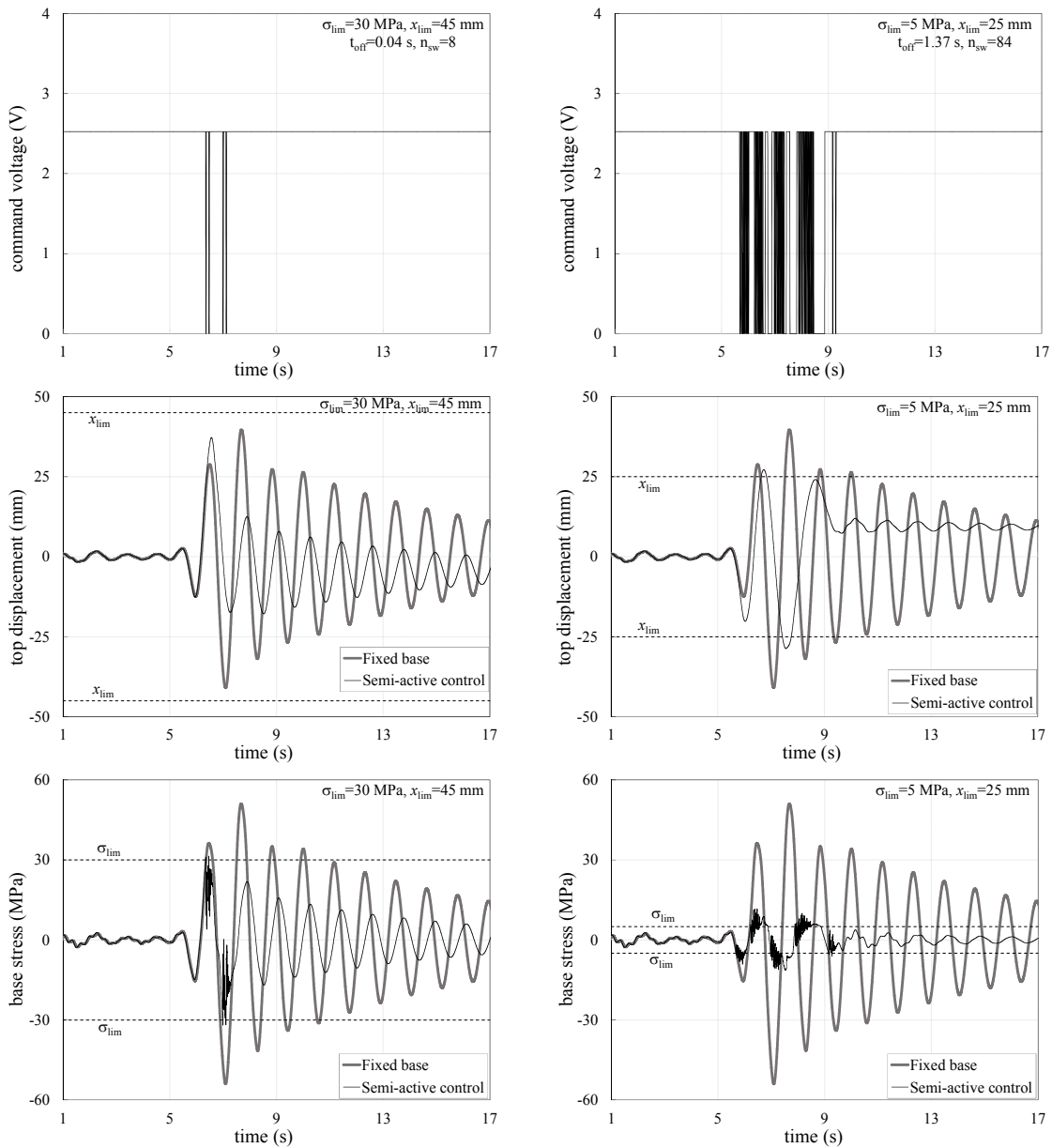


Fig. 9 Command voltage, base stress, and top displacement response time-histories for the cases  $(\sigma_{lim}, x_{lim})=(5 \text{ MPa}, 25 \text{ mm})$  and  $(\sigma_{lim}, x_{lim})=(30 \text{ MPa}, 45 \text{ mm})$

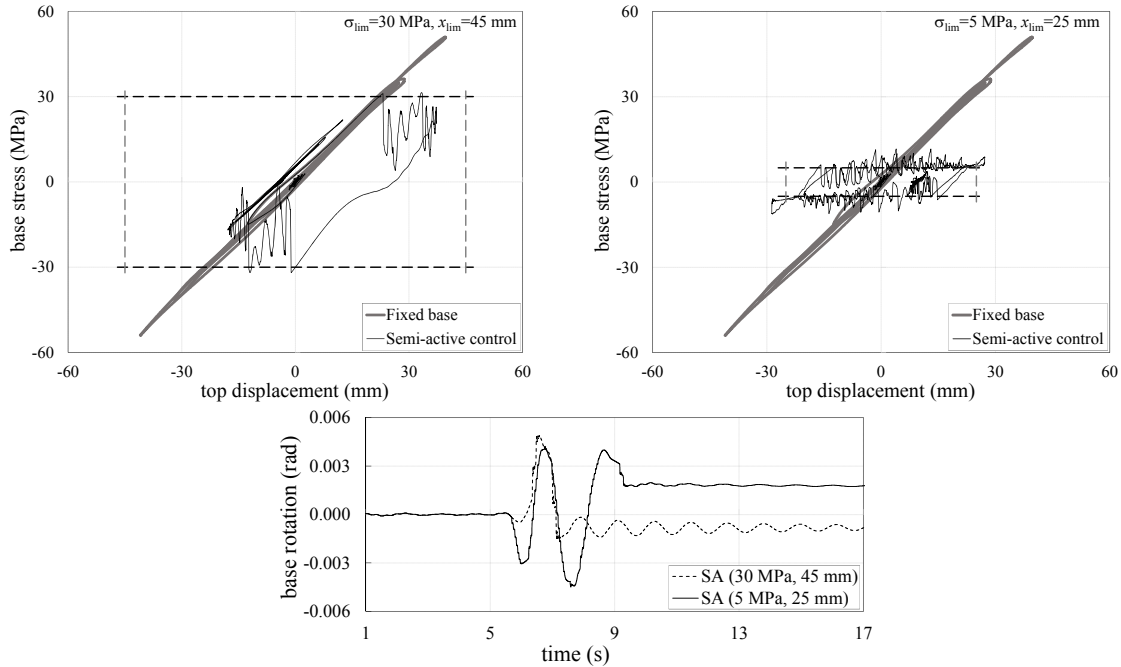


Fig. 10 Base stress-top displacement cycles and base rotation response time-histories for the selected cases  $(\sigma_{lim}, x_{lim})=(5$  MPa, 25 mm) and  $(\sigma_{lim}, x_{lim})=(30$  MPa, 45 mm)

Looking at the dashed rectangles in Figs. 10(a) and 10(b), whose semi-dimensions are  $\sigma_{lim}$  and  $x_{lim}$ , it is worth noting that all the  $\sigma$ - $x$  non-linear cycles result to be strictly inscribed in the said rectangle. This shows the high effectiveness of the SA control strategy in achieving the objective of “cutting” the response in correspondence of the assumed limit values for the two response parameters.

Finally, Fig. 10(c) shows a not negligible residual rotation of the base at the end of the loading history, especially for the case (5 MPa, 25 mm). The authors are studying how to improve the control algorithm so as to reduce this effect, eventually by recentering the tower at the end of the excitation or, better, periodically while it still acts on the structure.

## 5. Conclusions

The idea to instantaneously remote control base stiffness and damping of a wind tower to mitigate structural demand due to strong wind loads has been discussed herein. The reduction of stiffness at the base restraint itself would imply reduction of base bending moment, but at the cost of a significant, undesired increase of displacement demand at the top of the tower. This is no longer true when the change of stiffness is accompanied by a change of damping too. The greater rocking of the base can be not so harmful for displacement demand if it is coupled with a

significant dissipation of energy. This is the main concept the presented study is based on and that simulations herein discussed strongly confirm.

The semi-active control via magnetorheological dampers of a FE model of a wind turbine tower has been presented. The FE model has been validated through the results of a preliminary shaking table experimental campaign done with reference to such structure, physically realized at the laboratory of the Denmark Technical University in Copenhagen. The results of several numerical analyses allowed to draw significant comments about the way to calibrate a specific control algorithm designed for the purpose. The latter is based on two user-defined parameters, i.e. limit values for base stress  $\sigma_{lim}$  and top displacement  $x_{lim}$ . With reference to a specific wind load action, the optimal couple of values  $(\sigma_{lim}, x_{lim})$  has been found according to a calibration procedure. They result to be respectively about 10% and 50% of the corresponding peak response values ( $\sigma_{max,FB}$ ,  $x_{max,FB}$ ) of the fixed base reference case. They lead to time histories of both structural response parameters consistently included within these limits, with the exception of peak values that are around 20% of  $\sigma_{max,FB}$  and 70% of  $x_{max,FB}$  in that order. Moderately low values of  $\sigma_{lim}$  (25-50% of  $\sigma_{max,FB}$ ) led to increased top displacements, even higher than the reference value  $x_{max,FB}$ . A trend reversal for values of  $\sigma_{lim}$  even more smaller (10-20% of  $\sigma_{max,FB}$ ) has been registered, leading them to significant reduction of both base stress and top displacement, as said above, due to the higher operation of the controller and, consequently, to the sharp increase of dissipated energy due to the larger rocking of the base. Finally, the best configuration of the controller leads to very satisfactory results: about 80% and 30% of reduction respectively of base stress and top displacement in respect to the fixed base case.

The above results cannot be directly generalized, since dependent on the specific wind load case and turbine model assumed for the analyses. On the contrary, the conceptual findings they allowed to gather are always valid and will be exploited by the authors to program further investigations aimed at consolidating those outcomes and to finally determine the practical implications they could have. Further research about this topic will consider a larger set of wind load cases, different for magnitude, duration and frequency content, to understand if and how the optimal calibration of the control algorithm depends on the characteristics of the external action. Future developments should also be addressed to understand whether and how to reduce the residual top displacement due to the possible incremental base rotation that may happen during a wind load history, especially when it is long lasting. In other words, a possible way to give a recentering action (or actions) at the end of (or periodically during) the severe load history should be evaluated. Furthermore, the use of more realistic aerodynamic loading, rather than of equivalent base acceleration, will be explored. Finally, the possibility of changing the limit values  $\sigma_{lim}$ ,  $x_{lim}$  in real time according to the on-line measurement of one or more signals (e.g. wind velocity), representing wind load in that instant of time, could be explored.

## Acknowledgments

The Denmark Technical University (DTU) of Copenhagen is gratefully acknowledged for having financed the experimental activity, so giving the first input to the present research. The MR dampers have been designed, manufactured and provided for free by Maurer Söhne (Munich, Germany) that is also acknowledged for the support.

## References

- Basu, B., Staino, A. and Basu, M. (2014), "Role of flexible alternating current transmission systems devices in mitigating grid fault-induced vibration of wind turbines", *Wind Energy*, **17**, 1017-1033.
- Bortoluzzi, D., Casciati, S., Elia, L. and Faravelli, L. (2015), "Design of a TMD solution to mitigate wind-induced local vibrations in an existing timber footbridge", *Smart Struct. Syst.*, **16**(3), 459-478, doi: 10.12989/sss.2015.16.3.459.
- Caterino, N. (2015), "Semi-active control of a wind turbine via magnetorheological dampers", *J. Sound Vib.*, **345**, 1-17, doi:10.1016/j.jsv.2015.01.022.
- Caterino, N., Georgakis, C.T., Trinchillo, F. and Occhiuzzi, A. (2014), "A semi-active control system for wind turbines", In: N. Luo, Y. Vidal, L. Aho, *Wind Turbine Control and Monitoring*, Springer International Publishing, 375-407, Advances in Industrial Control, doi: 10.1007/978-3-319-08413-8\_13.
- Caterino, N., Spizzuoco, M. and Occhiuzzi, A. (2011), "Understanding and modelling the physical behaviour of magnetorheological dampers for seismic structural control", *Smart Mater. Struct.*, **20**(6), doi:10.1088/0964-1726/20/6/065013.
- Caterino, N., Spizzuoco, M. and Occhiuzzi, A. (2013), "Promptness and dissipative capacity of MR dampers: experimental investigations", *Struct. Control Health Monit.*, **20**(12), 1424-1440, doi: 10.1002/stc.1578.
- Chen, J. and Georgakis, C.T. (2013), "Tuned rolling-ball dampers for vibration control in wind turbines", *J. Sound Vib.*, **332**, 5271-5282, dx.doi.org/10.1016/j.jsv.2013.05.019.
- Chen, J. and Georgakis, C.T. (2015), "Spherical tuned liquid damper for vibration control in wind turbines", *J. Vib. Control*, **21**(10), 1875-1885, doi: 10.1177/1077546313495911.
- Colwell, S. and Basu, B. (2009), "Tuned liquid column dampers in offshore wind turbines for structural control", *Eng. Struct.*, **31**, 358-368, doi: 10.1016/j.engstruct.2008.09.001.
- Dinh, V.N. and Basu, B. (2015), "Passive control of floating offshore wind turbine nacelle and spar vibrations by multiple tuned mass dampers", *Struct. Control Health Monit.*, **22**(1), 152-176.
- Enevoldsen, I. and Mørk, K. (1996), "Effects of a vibration mass damper in a wind turbine tower", *Mech. Struct. Mach.*, **24**, 155-187.
- Karimi, H.R., Zapateiro, M. and Luo, N. (2010), "Semiactive vibration control of offshore wind turbine towers with tuned liquid column dampers using  $H_\infty$  output feedback control", *Proceedings of the IEEE International Conference on Control Applications*, Yokohama, Japan.
- Kirkegaard, P.H., Nielsen, S.R.K., Poulsen, B.L., Andersen, J., Pedersen, L.H. and Pedersen, B.J. (2002), *Semi-active vibration control of a wind turbine tower using an MR damper*, H. Grundmann, G.I. Schuëller, Rotterdam: Balkema Publishers, A.A. / Taylor & Francis The Netherlands, 1575-1580.
- Lackner, M. and Rotea, M. (2011), "Structural control of floating wind turbines", *Mechatronics*, **21**, 704-719, doi:10.1016/j.mechatronics.2010.11.007.
- Larsen, T.J. and Hansen, A.M. (2008), *HAWC2 User Manual*, Roskilde, Denmark: Risø National Laboratory, Technical University of Denmark.
- Li, J., Zhang, Z. and Chen, J. (2012), "Experimental study on vibration control of offshore wind turbines using a ball vibration absorber", *Energy Power Eng.*, **4**, 153-157, doi: 10.4236/epe.2012.43021.
- Luo, N., Bottasso, C.L., Karimi, H.R. and Zapateiro, M. (2011), "Semiactive Control for floating offshore wind turbines subject to aero-hydro dynamic loads", *Proceedings of the International Conference on Renewable Energies and Power Quality*, Las Palmas de Gran Canaria, Spain.
- Murtagh, P.J., Ghosh, A., Basu, B. and Broderick, B.M. (2008), "Passive control of wind turbine vibrations including blade/tower interaction and rotationally sampled turbulence", *Wind Energy*, **11**, 305-317, doi: 10.1002/we.249.
- Pedersen, A.S. (2012), "Safe operation and emergency shutdown of wind turbines", Master Thesis in 'Intelligent Autonomous Systems', Department of Electronic Systems, Aalborg University.
- Rodríguez, T.A., Carcangiu, C.E., Pineda, I., Fischer, T., Kuhnle, B., Scheu, M. and Martin, M. (2011), "Wind turbine structural damping control for tower load reduction", *Proceedings of the 29th IMAC, A Conference and Exposition on Structural Dynamics*, Jacksonville, FL, USA.

- Salvi, J. and Rizzi, E. (2016), "Closed-form optimum tuning formulas for passive Tuned Mass Dampers under benchmark excitations", *Smart Struct. Syst.*, **17**(2), 231-256, doi: 10.12989/sss.2016.17.2.231.
- Wisniewsky, R., Svenstrup, M., Pedersen, A.S. and Steiniche C.S. (2013), "Certificate for safe emergency shutdown of wind turbines", *Proceedings of the American Control Conference (ACC)*, 3667-3672, Washington, DC.
- Zhang, Z.L., Chen, J.B. and Li, J. (2013), "Theoretical study and experimental verification of vibration control of offshore wind turbines by a ball vibration absorber", *Struct. Infrastruct. Eng.*, **5**, doi.org/10.1080/15732479.2013.792098.